Int. J. Adv. Appl. Math. and Mech. 10(1) (2022) 28 – 38 (ISSN: 2347-2529)

Journal homepage: www.ijaamm.com

IJAAMM

International Journal of Advances in Applied Mathematics and Mechanics

Numerical Study on Turbulent Mixed Convection in a Greenhouse with Crop

Research Article

James Kigo*, **Mathew Kinyanjui**, **Roy Kiogora**

Department of Pure and Applied Mathematics, Jomo Kenyatta University of Agriculture and Technology, Juja, 62000-00200, Nairobi, Kenya

Received 23 August 2022; accepted (in revised version) 07 September 2022

Abstract: Mixed convection in a greenhouse with tomato crop is studied numerically with different aspect ratios. The effects of varying the ventilation size and position of the fan on the velocity and temperature profiles are determined. The low-Reynolds $k-\omega$ turbulence model is employed to close the governing equations. The partial differential equations governing the flow are discretized and solved by the finite volume method. It is found that increasing the Grashof number leads to an increase in velocity profiles and a decrease in the temperature profiles. Also, it is observed that increasing the inlet area, reducing the distance between the greenhouse floor and the fan and reducing the distance between greenhouse floor and the inlet reduce the temperature profiles. This study provides useful information that can aid greenhouse designers and operators to modify greenhouse ventilation for better thermal performance.

MSC: 76D05 • 76F10

Keywords: Greenhouse • Fan • Ventilation

1. Introduction

The greenhouse micro-climate is of importance as it affects the quality and quantity of the crops. Ventilation helps in maintaining a favourable greenhouse climate for optimal production. Mechanical,Natural or both mechanisms can be used for ventilation. The greenhouse temperatures are higher than the ambient temperatures which result in increase of water vapour deficits. Therefore, proper geometrical designs of greenhouses can help in improving the micro-climate for suitable crop growth. Numerical and experimental studies have been carried out by various researchers. [1] carried out a simulation on the microclimate of a naturally ventilated greenhouse using the Gembloux Greenhouse Dynamic Model (GGDM). They introduced the stomatal resistance of vegetation and the analysis showed that external wind speed and the opening angle of the vents significantly influenced the ventilation flux. [2] studied the effect of wind direction on climatic parameters inside a greenhouse. A naturally ventilated tunnel-type greenhouse was considered. Three different models were used i.e. the renormalisation group (RNG), realizable $k \sim \varepsilon$ model and the standard $k \sim \varepsilon$ model. It was observed that the wind direction influenced the temperature, velocity, and humidity distributions. The velocity field computed using the three different models showed noticeable difference in the temperature, velocity and humidity patterns in the greenhouse. This confirmed the importance of choice of the turbulence model.

[3] investigated natural ventilation in a plant free semi- arid greenhouse. Two single-span double-polyethylene greenhouses with high pressure fog nozzles roll-up side vents with insect screens and roof vent were constructed. The

* Corresponding author.
E-mail address(es): kigojamesm@gmail.com (James Kigo).

evaporation from the floor was considered to be negligible. A unique and simple control algorithm was proposed and tested. The tracer gas method was used to measure the natural ventilation rate continuously. It was observed that the relative humidity decreased with an increase in ventilation rate, and the water used for cooling increased. The control algorithm demonstrated the possibility of maintaining the relative humidity and temperature simultaneously within a desirable range while reducing water used in fog cooling. [4] simulated the climate in a multi-span and shark-fin shaped greenhouses. The effect of the wind speed were studied and compared by two-dimensional CFD. The top and the sides were equipped with roll up windows. It was observed that the air renewal rate was $27h^{-1}$ for the multi-span and $75h^{-1}$ for the shark-fin greenhouse at a wind speed of $4ms^{-1}$ with fully open windows. Also, the temperature profiles were more homogeneous inside the shark-fin greenhouse than in the multi-span greenhouse.

[5] investigated a greenhouse ventilation efficiency based on a two-dimensional CFD. The effect of roof vent and the wind on air flow and temperature distributions in a compartmentalised glasshouse was analysed numerically. The results showed that the opening configurations and wind speeds strongly affected the micro-climate parameters and the ventilation. Also, there are different micro-climate within each compartment due to the inside partition, which hinders air circulation between different parts of the greenhouse. [6] modelled (MICGREEN), which consisted of a set of algebraic equations where ambient temperature, solar radiations on earth's surface, soil temperature under the canopy, solar radiations on a normal surface, and soil temperature at 6cm depth were considered as model units. The Gauss-Seidal Iteration method was used to solve the equations. The outputs were inside air temperature, canopy temperature, cover temperature, and bare soil temperature. The numerical results were compared with the experimental results and agreement was found between the predicted and measured values.

[7] investigated natural ventilation in Amazcala and Zacatecas under hot conditions. Presence of the insect proof screens was taken into account by means of porous media approach. The inside temperature had a vertical distribution while it was constant on horizontal planes. The finite element method was used to solve the governing equations and it was observed that the ventilation in greenhouses due to temperature effect produces high exchange rates. [8] carried out an experimental study on the effects of wind on the flow patterns and microclimate of a mono-span greenhouse containing rose crops The greenhouse had two continuous side openings each side having an area of $3.2m^2$ one on the east wall and the other on the west wall. The results showed that wind flowing perpendicular to the greenhouse plane resulted in a cross-flow between the leeward and windward openings. The humidity and temperature ratio was higher near the roof than the crops, but the air velocity was higher near the crops than the roof.

[9] developed a mathematical model for an arch shaped greenhouse. The flow was unsteady, one dimensional and the thermal properties of the construction materials were time independent. Finite difference method was used to solve the equations. The results showed that increase in temperature was more if ambient temperature was less and increase was less if the ambient temperature was more. The predicted thermal environment helped in the selection of a crop nursery for growing. The predicted and experimental values were almost the same, with a variation of 2 to 3^0C. [10] carried out a comparison of five different single-span shapes of vinery, even-span, modified arch, uneven-span and Quonset. The flow was one-dimensional and quasi steady for every configuration. The width, length and height were kept the same for the five configurations. The internal reflection was ignored and the polyethylene considered was assumed not to diffuse light. Also, the curved surfaces in the Quonset and modified greenhouses were considered to be flat. The results showed that uneven span greenhouse receives maximum radiation while Quonset the minimum every month at all latitudes.

[11] investigated the aerodynamic study of the greenhouses. Computational fluid dynamics was used in this study, where round geometry and plane geometry were considered. The Effects of the wind velocity on pressure profiles were evaluated. It was observed that almost the entire roof was subjected to suction forces for the plane and round geometries. The results showed that for the round geometry, the forces were bigger than in plane geometry. However, there was bigger damage on plane geometry. It was concluded that flapping was the cause of the plastic tearing. [12] investigated natural and mechanical ventilation in a greenhouse using computational fluid dynamics. Three different configurations were considered where the first configuration had mechanical ventilators with a closed roof. The second and third configurations were both mechanically ventilated with 30% and 100% open roofs respectively. Different lengths were considered (28m, 50m, 75m and 100m) in the simulations. The results showed that roof ventilation improved the climate of the mechanically ventilated greenhouse. The exchange rate was increased by 22% and also there was climate uniformity because the greenhouse air mixed better. It was observed that increasing fan capacity reduced the temperature. However, the effect was less intense in greenhouses with open roof ventilators. Also the results showed that an enlarged inlet increased the system performance due to the elimination of backflow recirculation zones.

[13] modelled heat and mass exchange in a big-size greenhouse. The model was implemented in the MATLAB SIMULINK software. The simulations were used to carry out graphical and statistical validation of the model. Analysis of the simulated results was used to make statements of logical correctness of the model and also made it possible to determine the critical points of failure to adjust the developed model. [14]studied ventilation optimization of a solar greenhouse with removable back walls. Computational fluid dynamics was used in this study where a two dimensional transient simulation model was developed. The indoor airflow and temperature distributions in greenhouse with different back wall vent sizes were simulated. The results showed that the back wall vent of 1.4m increased the ventilation efficiency .Also, the average air temperature was reduced by approximately 1.7^0C and the highest dropped

by approximately 5.8^0C in comparison to the traditional solar greenhouse with the brick back wall.

[15] studied experimentally and numerically a mechanically ventilated greenhouse. A standard $k \sim \varepsilon$ model was used for CFD numerical study. An even span greenhouse was considered with a ventilation opening placed on the northern wall to reach the maximum cooling effect by using minimum ventilation. A hot summer environment with no wind was considered.The results showed that a good qualitative and quantative agreement was found between the experimental and numerical calculation with almost 20% for average difference of all the lines. [16]investigated a wind-driven natural ventilation in a greenhouse with screens. Computational fluid dynamics simulations of ventilation in a greenhouse with and without screens was performed by finite volume method with $k \sim \varepsilon$ turbulence model. The validation was done by a comparison with velocity measurements from a greenhouse owned by the Bologna University. The results showed that the screens strongly affected the airflow velocity distribution and flow rates through the vents. For the case with screens a more uniform distributions of velocity field was observed than the case without screens.

[17]studied the effectiveness of ridge vent to wind-driven ventilation in a mono-slope multi-span greenhouse. A three-dimensional LES simulation model and wind tunnel experiments were used. The numerical results were validated using the experimental results. In addition an analytical model was used to compute the ventilation rate. The study showed that the ventilation rates of the greenhouse with open ridge vents were much higher than that of greenhouse with closed ridge vents. Also, the windward ridge vent substantially increased the ventilation rate compared to leeward ridge vent. [18] studied the effect of increasing ventilation area on airflow patterns and thermal distribution in a traditional Colombian greenhouse using computational fluid dynamics. A passively ventilated greenhouse was considered and a numerical model was developed using two-dimensional CFD which was validated experimentally. The study showed that increase in roof ventilation areas reduced the averaged internal temperatures by up to 16%. The temperature homogeneity was improved and ventilation rate were increased by 19% with respect to the referenced scenario. [19]investigated numerically and experimentally the thermal performance of evaporative cooled greenhouse in hot and arid climates. Three design factors namely: greenhouse geometry, geographical location and operational parameters were assessed. CFD was used to model ASHRAE compliant greenhouse. The results showed that doubling the ventilation rate further decreased the air temperature. Although many investigations have been made on greenhouses, only a few consider three dimensional greenhouse. An adequate comprehension of mixed convection in a greenhouse with crops is essential to redesign ventilation systems of greenhouses. The objective of this paper is to investigate the effect of varying fan position, inlet area and inlet position on the velocity and temperature profiles. The non-dimensional governing equations are solved by the finite volume method.

2. Mathematical formulation

We consider a 3D transient turbulent flow of an incompressible fluid with variable viscosity and thermal conductivity in a greenhouse. The greenhouse roof is assumed to be horizontal and the walls are adiabatic except the bottom wall which is isothermal. A fan is placed at the right wall and an inlet at the left wall as shown in Fig. 1. Á Cartesian coordinate system (x, y, z) is chosen where; x-direction is taken to be the length,y-direction is the width and z-direction is the height of the greenhouse. The greenhouse contain mature tomato crop which drag the airflow and also release

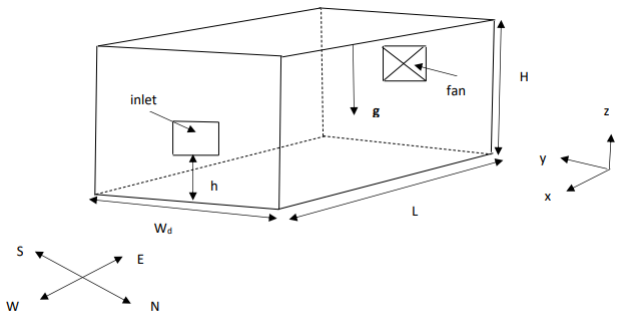

Fig. 1. Geometry of the problem

heat during the transpiration. The drag force per crop volume as recommended by [19] is given by

$$D = -\rho I_{LAD} C_d U^2 \tag{1}$$

Where ρ is the density of air,I_{LAD} is the leaf area density, C_d the crop drag coefficient and U is the velocity vector of air. During transpiration the crop release sensible heat which is given by [20]

$$Q_{sen} = \frac{I_{LA}\rho c_p\left(\bar{T_w} - \bar{T}\right)}{r_a} \tag{2}$$

Where I_{LA} is crop stand leaf area index, c_p is the specific heat at constant pressure, r_a is the aerodynamic resistance, $\overline{T}$ is the averaged temperature and $\overline{T}_w$ is the wall temperature. Under the assumptions and taking into consideration the crop drag force and the sensible heat released, the time-averaged Navier–Stokes equations for unsteady turbulent mixed convection after invoking the Boussinesq approximation and neglecting the viscous dissipation are expressed as:

$$\frac{\partial \bar{u}}{\partial x} + \frac{\partial \bar{v}}{\partial y} + \frac{\partial \bar{w}}{\partial z} = 0 \tag{3}$$

$$\begin{aligned}\rho\frac{\partial \overline{u}}{\partial t} + \rho\left(\overline{u}\frac{\partial \overline{u}}{\partial x} + \overline{v}\frac{\partial \overline{u}}{\partial y} + \overline{w}\frac{\partial \overline{u}}{\partial z}\right) &= -\frac{\partial \overline{p}}{\partial x} + \frac{\partial}{\partial x}\left(\mu\frac{\partial \overline{u}}{\partial x}\right) + \frac{\partial}{\partial y}\left(\mu\frac{\partial \overline{u}}{\partial y}\right) + \frac{\partial}{\partial z}\left(\mu\frac{\partial \overline{u}}{\partial z}\right) - \rho I_{LAD}C_d\overline{u}^2 \\ &- \frac{\partial}{\partial x}\left(\rho\overline{u'^2}\right) - \frac{\partial}{\partial y}\left(\rho\overline{u'v'}\right) - \frac{\partial}{\partial z}\left(\rho\overline{u'w'}\right)\end{aligned} \tag{4}$$

$$\begin{aligned}\rho\frac{\partial \overline{v}}{\partial t} + \rho\left(\overline{u}\frac{\partial \overline{v}}{\partial x} + \overline{v}\frac{\partial \overline{v}}{\partial y} + \overline{w}\frac{\partial \overline{v}}{\partial z}\right) &= -\frac{\partial \overline{p}}{\partial y} + \frac{\partial}{\partial x}\left(\mu\frac{\partial \overline{v}}{\partial x}\right) + \frac{\partial}{\partial y}\left(\mu\frac{\partial \overline{v}}{\partial y}\right) + \frac{\partial}{\partial z}\left(\mu\frac{\partial \overline{v}}{\partial z}\right) - \rho I_{LAD}C_d\overline{v}^2 \\ &- \frac{\partial}{\partial x}\left(\rho\overline{u'v'}\right) - \frac{\partial}{\partial y}\left(\rho\overline{v'^2}\right) - \frac{\partial}{\partial z}\left(\rho\overline{v'w'}\right)\end{aligned} \tag{5}$$

$$\begin{aligned}\rho\frac{\partial \overline{w}}{\partial t} + \rho\left(\overline{u}\frac{\partial \overline{w}}{\partial x} + \overline{v}\frac{\partial \overline{w}}{\partial y} + \overline{w}\frac{\partial \overline{w}}{\partial z}\right) &= -\frac{\partial \overline{p}}{\partial z} + \frac{\partial}{\partial x}\left(\mu\frac{\partial \overline{w}}{\partial x}\right) + \frac{\partial}{\partial y}\left(\mu\frac{\partial \overline{w}}{\partial y}\right) + \frac{\partial}{\partial z}\left(\mu\frac{\partial \overline{w}}{\partial z}\right) - \rho I_{LAD}C_d\overline{w}^2 \\ &+ \rho_\infty g\beta(\overline{T} - T_\infty) - \frac{\partial}{\partial x}\left(\rho\overline{u'w'}\right) - \frac{\partial}{\partial y}\left(\rho\overline{v'w'}\right) - \frac{\partial}{\partial z}\left(\rho\overline{w'^2}\right)\end{aligned} \tag{6}$$

$$\begin{aligned}\rho c_p\left(\frac{\partial \overline{T}}{\partial t} + \overline{u}\frac{\partial \overline{T}}{\partial x} + \overline{v}\frac{\partial \overline{T}}{\partial y} + \overline{w}\frac{\partial \overline{T}}{\partial z}\right) &= \frac{\partial}{\partial x}\left(\kappa\frac{\partial \bar{T}}{\partial x}\right) + \frac{\partial}{\partial y}\left(\kappa\frac{\partial \bar{T}}{\partial y}\right) + \frac{\partial}{\partial z}\left(\kappa\frac{\partial \bar{T}}{\partial z}\right) + I_{LA}\rho c_p(\overline{T}_w - \overline{T})/r_a \\ &- \frac{\partial}{\partial x}(\rho c_p\overline{u'T'}) - \frac{\partial}{\partial y}(\rho c_p\overline{v'T'}) - \frac{\partial}{\partial z}(\rho c_p\overline{w'T'})\end{aligned} \tag{7}$$

Where $\overline{u}$, $\overline{v}$ and $\overline{w}$ are the averaged velocities, $\overline{p}$ averaged pressure, ρ is the density, g the gravitational force in vertical direction z, C_d is the crop drag force coefficient. To close the governing equations appropriate dependence laws of conductivity and viscosity are introduced. According to [21]and [22],

$$\kappa(T) = \kappa_\infty\left[1 + c\left(\overline{T} - T_\infty\right)\right] \tag{8}$$

and

$$\frac{1}{\mu} = \frac{1}{\mu_\infty}[1 + \gamma(\overline{T} - T_\infty)] \tag{9}$$

respectively. The set of equations are simplified by employing the Boussinesq approximation. The turbulent stresses in equations(4 - 6) and turbulent heat flux in equation 7 are derived from the turbulence closure model.

$$-\rho\overline{u_i'u_j'} = 2\mu_t S_{ij} - \frac{2}{3}\rho k\delta_{ij} \tag{10}$$

and

$$-\rho c_p\overline{T'u_j'} = c_p\frac{\mu_t}{pr_t}\frac{\partial \overline{T}}{\partial x_j} \tag{11}$$

Where $S_{ij} = \frac{1}{2}[\frac{\partial \overline{u}_i}{\partial x_j} + \frac{\partial \overline{u}_j}{\partial x_i}]$ the mean stress tensor, μ_t is the turbulent viscosity, pr_t is the turbulent prandtl number, δ_{ij} isthe Kronecker delta and k is the turbulent kinetic energy given as

$$k = \frac{1}{2}(\overline{u}^2 + \overline{v}^2 + \overline{w}^2) \tag{12}$$

for a three dimensional problem. Thus, substituting the turbulent stresses and turbulent heat fluxes equations (4-7) simplifies to

$$\rho\left[\frac{\partial\bar{u}}{\partial t}+\bar{u}\frac{\partial\bar{u}}{\partial x}+\bar{v}\frac{\partial\bar{u}}{\partial y}+\bar{w}\frac{\partial\bar{u}}{\partial z}\right]=-\frac{\partial\bar{p}}{\partial x}+\frac{\partial}{\partial x}\left[\left(\frac{\mu_\infty}{1+\gamma\left(\bar{T}-T_\infty\right)}+\mu_t\right)\frac{\partial\bar{u}}{\partial x}\right]$$
$$+\frac{\partial}{\partial y}\left[\left(\frac{\mu_\infty}{1+\gamma\left(\bar{T}-T_\infty\right)}+\mu_t\right)\frac{\partial\bar{u}}{\partial y}\right]+\frac{\partial}{\partial z}\left[\left(\frac{\mu_\infty}{1+\gamma\left(\bar{T}-T_\infty\right)}+\mu_t\right)\frac{\partial\bar{u}}{\partial z}\right] \tag{13}$$
$$-I_{LAD}\rho C_d\bar{u}^2$$

$$\rho\left[\frac{\partial\bar{v}}{\partial t}+\bar{u}\frac{\partial\bar{v}}{\partial x}+\bar{v}\frac{\partial\bar{v}}{\partial y}+\bar{w}\frac{\partial\bar{v}}{\partial z}\right]=-\frac{\partial\bar{p}}{\partial y}+\frac{\partial}{\partial x}\left[\left(\frac{\mu_\infty}{1+\gamma\left(\bar{T}-T_\infty\right)}+\mu_t\right)\frac{\partial\bar{v}}{\partial x}\right]$$
$$+\frac{\partial}{\partial y}\left[\left(\frac{\mu_\infty}{1+\gamma\left(\bar{T}-T_\infty\right)}+\mu_t\right)\frac{\partial\bar{v}}{\partial y}\right]+\frac{\partial}{\partial z}\left[\left(\frac{\mu_\infty}{1+\gamma\left(\bar{T}-T_\infty\right)}+\mu_t\right)\frac{\partial\bar{v}}{\partial z}\right] \tag{14}$$
$$-I_{LAD}\rho C_d\bar{v}^2$$

$$\rho\left[\frac{\partial\bar{w}}{\partial t}+\bar{u}\frac{\partial\bar{w}}{\partial x}+\bar{v}\frac{\partial\bar{w}}{\partial y}+\bar{w}\frac{\partial\bar{w}}{\partial z}\right]=-\frac{\partial\bar{p}}{\partial z}+\frac{\partial}{\partial x}\left[\left(\frac{\mu_\infty}{1+\gamma\left(\bar{T}-T_\infty\right)}+\mu_t\right)\frac{\partial\bar{w}}{\partial x}\right]$$
$$+\frac{\partial}{\partial y}\left[\left(\frac{\mu_\infty}{1+\gamma\left(\bar{T}-T_\infty\right)}+\mu_t\right)\frac{\partial\bar{w}}{\partial y}\right]+\frac{\partial}{\partial z}\left[\left(\frac{\mu_\infty}{1+\gamma\left(\bar{T}-T_\infty\right)}+\mu_t\right)\frac{\partial\bar{w}}{\partial z}\right] \tag{15}$$
$$-I_{LAD}\rho C_d\bar{w}^2+\rho_\infty g\beta\left(\bar{T}-T_\infty\right)$$

$$\rho c_p\left[\frac{\partial\bar{T}}{\partial t}+\bar{u}\frac{\partial\bar{T}}{\partial x}+\bar{v}\frac{\partial\bar{T}}{\partial y}+\bar{w}\frac{\partial\bar{T}}{\partial z}\right]=\frac{\partial}{\partial x}\left[\kappa_\infty\left(1+c\left(\bar{T}-T_\infty\right)+\rho c_p\Gamma_t\right)\frac{\partial\bar{T}}{\partial x}\right]+$$
$$\frac{\partial}{\partial y}\left[\kappa_\infty\left(1+c\left(\bar{T}-T_\infty\right)+\rho c_p\Gamma_t\right)\frac{\partial\bar{T}}{\partial y}\right]+\frac{\partial}{\partial z}\left[\kappa_\infty\left(1+c\left(\bar{T}-T_\infty\right)+\rho c_p\Gamma_t\right)\frac{\partial\bar{T}}{\partial z}\right]+ \tag{16}$$
$$\frac{I_{LA}\rho C_p\left(\bar{T}_w-\bar{T}\right)}{r_a}$$

The $k-\omega$ model [23] is employed for solving the closure problem. Where

$$\mu_t=\frac{\rho k}{\omega} \tag{17}$$

and

$$\Gamma_t=\frac{\mu_t}{pr_t} \tag{18}$$

3. Boundary Conditions

The boundary conditions for the above model are as follows:
for $t\le 0$:
$\overline{u}=\overline{v}=\overline{w}=\overline{T}=0$
and for $t>0$:
At the walls we have:
$\overline{u}=\overline{v}=\overline{w}=0$ at $x=0$ and at $x=L$
$\overline{u}=\overline{v}=\overline{w}=0$ at $y=0$ and at $x=W_d$
$\overline{u}=\overline{v}=\overline{w}=0$ at $z=0$ and at $z=H$
$\overline{T}=T_w$ at the bottom wall
$\frac{\partial\overline{T}}{\partial n}=0$ at the adiabatic walls
At the inlet
$\overline{u}=u_\infty$, $\overline{v}=\overline{w}=0$, $\overline{T}=T_\infty$
At the oulet
$\overline{u}=u_f$, $\overline{v}=\overline{w}=0$, $\frac{\partial\overline{T}}{\partial n}=0$

4. Nondimensionalization

The following transformations are used to non-dimensionalize the set of governing equations.

$$x^\star = \frac{x}{L}, y^\star = \frac{y}{L}, z^\star = \frac{z}{L}, \bar{u}^\star = \frac{\bar{u}}{u_0}, \bar{v}^\star = \frac{\bar{v}}{u_0}, \bar{w}^\star = \frac{\bar{w}}{u_0}, t^\star = \frac{u_0}{L}t, \bar{p}^\star = \frac{\bar{p}}{\rho u_0^2},$$
$$\bar{T}^\star = \frac{\bar{T} - T_\infty}{\bar{T}_w - T_\infty}, \mu_t^\star = \frac{\mu_t}{\mu_\infty} \tag{19}$$

Using equation 19, equations (13-16) become

$$\frac{\partial \bar{u}}{\partial t} + \frac{\partial(\bar{u}\bar{u})}{\partial x} + \frac{\partial(\bar{u}\bar{v})}{\partial y} + \frac{\partial(\bar{u}\bar{w})}{\partial z} = -\frac{\partial \bar{p}}{\partial x} + \frac{\partial}{\partial x}\left[\left(\frac{1}{Re\left(1+a\bar{T}\right)} + \frac{\mu_t}{Re}\right)\frac{\partial \bar{u}}{\partial x}\right]$$
$$+ \frac{\partial}{\partial y}\left[\left(\frac{1}{Re\left(1+a\bar{T}\right)} + \frac{\mu_t}{Re}\right)\frac{\partial \bar{u}}{\partial y}\right] + \frac{\partial}{\partial z}\left[\left(\frac{1}{Re\left(1+a\bar{T}\right)} + \frac{\mu_t}{Re}\right)\frac{\partial \bar{u}}{\partial z}\right] - I_{LAD}C_d L\bar{u}^2 \tag{20}$$

$$\frac{\partial \bar{v}}{\partial t} + \frac{\partial(\bar{v}\bar{u})}{\partial x} + \frac{\partial(\bar{v}\bar{v})}{\partial y} + \frac{\partial(\bar{v}\bar{w})}{\partial z} = -\frac{\partial \bar{p}}{\partial y} + \frac{\partial}{\partial x}\left[\left(\frac{1}{Re\left(1+a\bar{T}\right)} + \frac{\mu_t}{Re}\right)\frac{\partial \bar{v}}{\partial x}\right]$$
$$+ \frac{\partial}{\partial y}\left[\left(\frac{1}{Re\left(1+a\bar{T}\right)} + \frac{\mu_t}{Re}\right)\frac{\partial \bar{v}}{\partial y}\right] + \frac{\partial}{\partial z}\left[\left(\frac{1}{Re\left(1+a\bar{T}\right)} + \frac{\mu_t}{Re}\right)\frac{\partial \bar{v}}{\partial z}\right] - I_{LAD}C_d L\bar{v}^2 \tag{21}$$

$$\frac{\partial \bar{w}}{\partial t} + \frac{\partial(\bar{w}\bar{u})}{\partial x} + \frac{\partial(\bar{w}\bar{v})}{\partial y} + \frac{\partial(\bar{w}\bar{w})}{\partial z} = -\frac{\partial \bar{p}}{\partial z} + \frac{\partial}{\partial x}\left[\left(\frac{1}{Re\left(1+a\bar{T}\right)} + \frac{\mu_t}{Re}\right)\frac{\partial \bar{w}}{\partial x}\right]$$
$$+ \frac{\partial}{\partial y}\left[\left(\frac{1}{Re\left(1+a\bar{T}\right)} + \frac{\mu_t}{Re}\right)\frac{\partial \bar{w}}{\partial y}\right] + \frac{\partial}{\partial z}\left[\left(\frac{1}{Re\left(1+a\bar{T}\right)} + \frac{\mu_t}{Re}\right)\frac{\partial \bar{w}}{\partial z}\right] - I_{LAD}C_d L\bar{w}^2 + \frac{Gr}{Re^2}\bar{T} \tag{22}$$

$$\frac{\partial \bar{T}}{\partial t} + \frac{\partial\left(\bar{u}\bar{T}\right)}{\partial x} + \frac{\partial\left(\bar{v}\bar{T}\right)}{\partial y} + \frac{\partial\left(\bar{w}\bar{T}\right)}{\partial z} = \frac{\partial}{\partial x}\left[\left(\frac{1+b\bar{T}}{PrRe} + \frac{\mu_t}{Pr_tRe}\right)\frac{\partial \bar{T}}{\partial x}\right] + \frac{\partial}{\partial y}\left[\left(\frac{1+b\bar{T}}{PrRe} + \frac{\mu_t}{Pr_tRe}\right)\frac{\partial \bar{T}}{\partial y}\right]$$
$$+ \frac{\partial}{\partial z}\left[\left(\frac{1+b\bar{T}}{PrRe} + \frac{\mu_t}{Pr_tRe}\right)\frac{\partial \bar{T}}{\partial z}\right] + \frac{I_{LA}L\left(1-\bar{T}\right)}{u_0 r_a} \tag{23}$$

The boundary conditions in non-dimensional form are given by:
for $t \leq = 0$:
$\overline{u} = \overline{v} = \overline{w} = \overline{T} = 0$
and for $t > 0$:
At the walls we have:
$\overline{u} = \overline{v} = \overline{w} = 0$ at $x = 0$ and at $x = L$
$\overline{u} = \overline{v} = \overline{w} = 0$ at $y = 0$ and at $x = W_d$
$\overline{u} = \overline{v} = \overline{w} = 0$ at $z = 0$ and at $z = H$
$\overline{T} = 1$ at the bottom wall
$\frac{\partial \overline{T}}{\partial n} = 0$ at the adiabatic walls
At the inlet
$\overline{u} = 1$, $\overline{v} = \overline{w} = 0$, $\overline{T} = 0$
At the oulet
$\overline{u} = u_f$, $\overline{v} = \overline{w} = 0$, $\frac{\partial \overline{T}}{\partial n} = 0$
The non-dimensional numbers obtained are $Re = \frac{\rho u_0 L}{\mu_\infty}$ is the Reynolds number, $Ri = \frac{Gr}{Re^2}$ is the Richardson number, $Gr = \frac{g\beta L^3(\bar{T}_w - T_\infty)}{u_0^2}$ is the Grashof number, $Pr = \frac{\mu_\infty c_p}{k_\infty}$ is the prandtl number. The variable viscosity parameter is $\gamma < 0$ and $a = \gamma(\bar{T}_w - T_\infty)$. $c > 0$ represent the variable thermal conductivity parameter and $b = c\,(T - T_\infty)$

5. Numerical approach

The governing equations are solved using the finite volume method [24]. The domain is divided into control volumes and the governing equations are discretized by integrating over each sub-domain. The control volume has a centre node P surrounded by six other nodes identified as west, east, south, north, bottom and top with the notations W, E, S, N, B and T respectively. The cell faces have the notations w, e, s, n, b and t referring to west, east, south, north, bottom and top faces respectively. The distances between the nodes P and E, W and P, P and N, S and P, P and T, B

and P are denoted by δx_{PE}, δx_{WP}, δy_{PN},δy_{SP}, δz_{PT}, and δz_{BP} respectively. The distances between the east and west, north and south and top and bottom faces are respectively Δx, Δy and Δz.

By employing this technique the discretized governing equations are as follows. The x-direction momentum equation is,

$$a_P u_p = a_E u_E + a_W u_W + a_N u_N + a_S u_S + a_T u_T + a_B u_B + a_P^0 u_P^0 + S_u + \Delta p \tag{24}$$

Where $a_P = a_P^0 + a_E + a_W + a_N + a_S + a_T + a_B - S_P$ $a_P^0 = \frac{\Delta x}{\Delta t}$, $a_E = \left(\frac{N_e}{\delta x_{PE}} - \frac{u_e}{2}\right)$, $a_W = \left(\frac{N_w}{\delta x_{WP}} + \frac{u_w}{2}\right)$, $a_N = \left(\frac{N_n}{\delta y_{PN}} - \frac{v_n}{2}\right)$, $a_S = \left(\frac{N_s}{\delta y_{SP}} + \frac{v_s}{2}\right)$, $a_T = \left(\frac{N_t}{\delta z_{PT}} - \frac{w_t}{2}\right)$,

$a_B = \left(\frac{N_b}{\delta z_{BP}} + \frac{w_b}{2}\right)$, $S_P = -2I_{LAD}C_d L\Delta x u_P^0$, $S_u = I_{LAD}C_d L\Delta x u_P^0$, $\Delta p = \frac{p_E}{2} - \frac{p_W}{2}$
Similarly the discretized y-direction equation is

$$a_P v_p = a_E v_E + a_W v_W + a_N v_N + a_S v_S + a_T v_T + a_B v_B + a_P^0 v_P^0 + S_u + \Delta p \tag{25}$$

Where
$a_P = a_P^0 + a_E + a_W + a_N + a_S + a_T + a_B - S_P$
$a_P^0 = \frac{\Delta y}{\Delta t}$, $a_E = \left(\frac{N_e}{\delta x_{PE}} - \frac{u_e}{2}\right)$, $a_W = \left(\frac{N_w}{\delta x_{WP}} + \frac{u_w}{2}\right)$, $a_N = \left(\frac{N_n}{\delta y_{PN}} - \frac{v_n}{2}\right)$, $a_S = \left(\frac{N_s}{\delta y_{SP}} + \frac{v_s}{2}\right)$,
$a_T = \left(\frac{N_t}{\delta z_{PT}} - \frac{w_t}{2}\right)$, $a_B = \left(\frac{N_b}{\delta z_{BP}} + \frac{w_b}{2}\right)$, $S_P = -2I_{LAD}C_d L\Delta y v_P^0$, $S_u = I_{LAD}C_d L\Delta y v_P^0$, $\Delta p = \frac{p_N}{2} - \frac{p_S}{2}$,
Similarly the discretized z-direction momentum equation is

$$a_P w_p = a_E w_E + a_W w_W + a_N w_N + a_S w_S + a_T w_T + a_B w_B + a_P^0 w_P^0 + S_u + \Delta p + Ri T_P^0 \tag{26}$$

Where
$a_P = a_P^0 + a_E + a_W + a_N + a_S + a_T + a_B - S_P$
$a_P^0 = \frac{\Delta z}{\Delta t}$ $a_E = \left(\frac{N_e}{\delta x_{PE}} - \frac{u_e}{2}\right)$ $a_W = \left(\frac{N_w}{\delta x_{WP}} + \frac{u_w}{2}\right)$ $a_N = \left(\frac{N_n}{\delta y_{PN}} - \frac{v_n}{2}\right)$ $a_S = \left(\frac{N_s}{\delta y_{SP}} + \frac{v_s}{2}\right)$ $a_T = \left(\frac{N_t}{\delta z_{PT}} - \frac{w_t}{2}\right)$
$a_B = \left(\frac{N_b}{\delta z_{BP}} + \frac{w_b}{2}\right)$ $S_P = -2I_{LAD}C_d L\Delta z w_P^0$ $S_u = I_{LAD}C_d L\Delta z w_P^0$ $\Delta p = \frac{p_T}{2} - \frac{p_B}{2}$
Similarly the discretized energy equation is

$$a_P T_p = a_E T_E + a_W T_W + a_N T_N + a_S T_S + a_T T_T + a_B T_B + a_P^0 T_P^0 + S_u \tag{27}$$

Where $a_P = a_P^0 + a_E + a_W + a_N + a_S + a_T + a_B - S_P$
$a_P^0 = \frac{\Delta x}{\Delta t}$ $a_E = \left(\frac{M_e}{\delta x_{PE}} - \frac{u_e}{2}\right)$ $a_W = \left(\frac{M_w}{\delta x_{WP}} + \frac{u_w}{2}\right)$ $a_N = \left(\frac{M_n}{\delta y_{PN}} - \frac{v_n}{2}\right)$ $a_S = \left(\frac{M_s}{\delta y_{SP}} + \frac{v_s}{2}\right)$ $a_T = \left(\frac{M_t}{\delta z_{PT}} - \frac{w_t}{2}\right)$
$a_B = \left(\frac{M_b}{\delta z_{BP}} + \frac{w_b}{2}\right)$ $S_P = \frac{I_{LA}L}{u_0 r_a}\Delta z$ $S_u = \frac{\Delta x}{\Delta t} T_P^0 \frac{I_{LA}L}{u_0 r_a}\Delta z$

6. Results and Discussions

Numerical computations are performed and the effects of varying fan position, air inlet position and inlet area on the fluid flow within a three-dimensional greenhouse are presented graphically and discussed. The results are analyzed in terms of velocity and temperature profiles over a wide range of Grashof number ($10e5 \le Gr \le 10e7$) and the aspect ratio ($1 \le AR \le 2$). The working fluid is air with Prandtl number $Pr = 0.71$ and the aspect ratio $AR = \frac{H}{L}$. The effects of varying Grashof number, air inlet area and fan and air inlet position on the velocity and temperature profiles are shown in figures (2-11)

Velocity and Temperature profiles

Figures (2-4) show the influence of Grashof number on the velocity profiles. Grashof number is the ratio of buoyancy forces to viscous forces and represents the effect of free convective currents. It is observed that as the Grashof number increase, the velocity profiles increase. This increase is attributed by the enhancement of the buoyancy forces. Figure 5 represents the velocity surface plot and it is observed that the velocities are zero at the walls and increase towards the centre of the greenhouse. It depicts the same behaviour of the velocities as in the velocity profiles. Figure 6 shows the influence of Prandtl number on the temperature profiles. The Prandtl number is the ratio of momentum to thermal diffusivity. It is observed that as the Prandtl number increase the temperature profiles increase. An increase in the Prandtl Number indicates a decrease in the fluid's thermal diffusivity, which leads to an increase in the fluid's internal temperature. Figure 7 shows the influence of Grashof number on the temperature profiles. It is observed that an increase in Grashof number leads to a decrease in temperature profiles. This is due to the fact that the thermal boundary layer thickness decrease as Grashof number increase. Figure 8 shows the effect of varying the fan position along the vertical distance. It is observed that as the distance between the greenhouse floor and the fan position decrease, the temperature profiles decrease. Figure 9 shows the effect of increasing the inlet area(A) on the temperature.

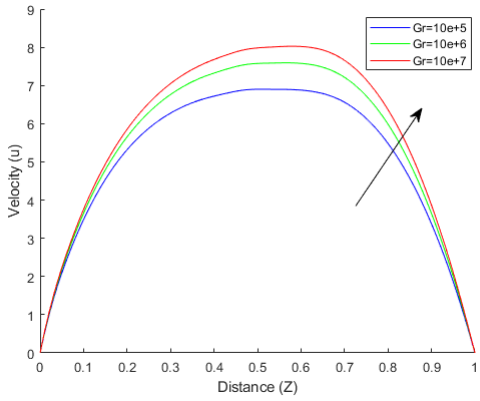

Fig. 2. The Velocity profiles for various values of Gr at X=0.5,Y=0.5 with Re=10,000, Pr=0.71 and AR=1

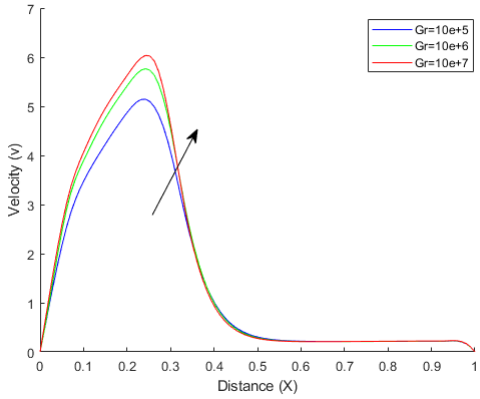

Fig. 3. The Velocity profiles for various values of Gr at Y=0.5,Z=0.5 with Re=10,000, Pr=0.71 and AR=1

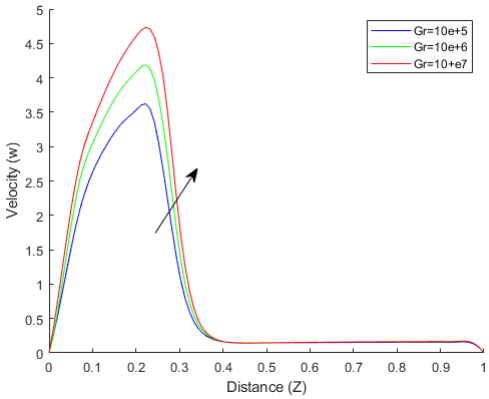

Fig. 4. The Velocity profiles for various values of Gr at X=0.5,Y=0.5 with Re=10,000, Pr=0.71 and AR=1

It is observed that increasing the inlet area reduces the greenhouse averaged temperature. As the inlet area increases larger amounts of colder air enters the greenhouse resulting in decrease in internal temperature. Figure 10 shows the effect of varying the inlet position along the vertical distance on the greenhouse climate. It is observed that the inside temperature decrease as the inlet distance from the greenhouse floor decrease. Figure 11 shows the temperature surface plot with the observation that the temperatures are highest at the bottom wall. As the greenhouse height increase the temperature decrease. The temperature surface plot is in an agreement with the temperature profiles.

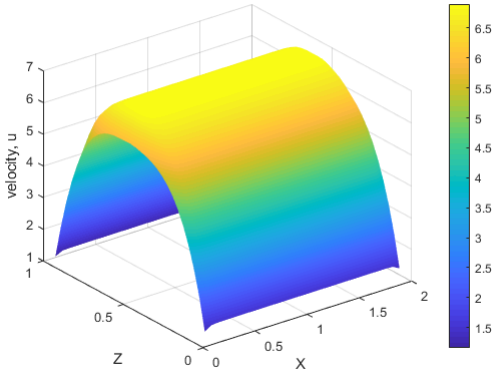

Fig. 5. The Velocity surface plot at Y=0.5 with Re=10,000, Pr=0.71, Gr=10^6 and AR=0.5

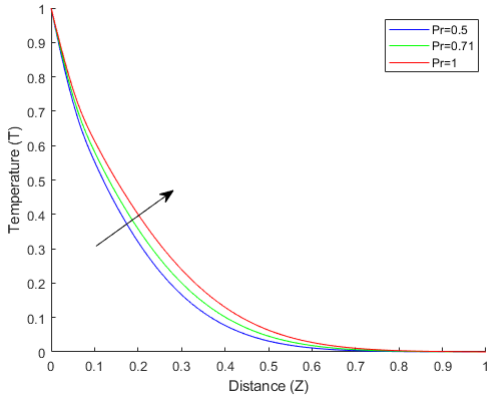

Fig. 6. The Temperature profiles for various values of Pr at X=0.5,Y=0.5 with Re=10,000, Pr=0.71, Gr=10^6 and AR=1

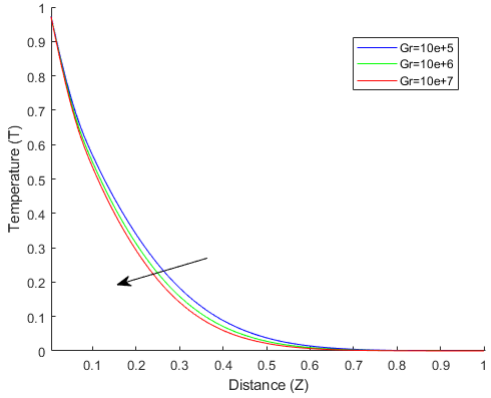

Fig. 7. The Temperature profiles for various values of Gr at X=0.5,Y=0.5 with Re=10,000, Pr=0.71, Gr=10^6 and AR=1

7. Conclusion

Transient 3D turbulent mixed convection in a greenhouse with a horizontal roof containing mature tomato crop is carried out in this study. The effects of varying various parameters are determined and observations summarized as follows.

1 . Velocity components are increasing functions of Grashof number. However the temperature decrease with an increase in Grashof number.

2 . An increase in the inlet area leads to a decrease in temperature profiles.

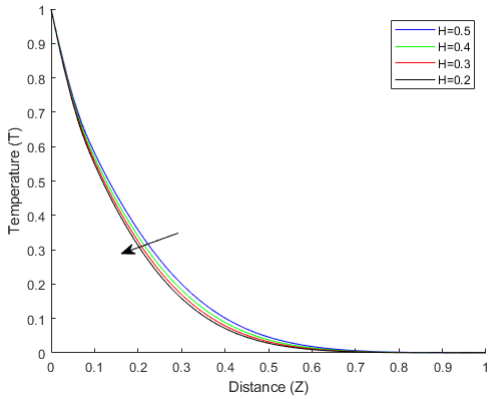

Fig. 8. The Temperature profiles for various values of H at X=0.5,Y=0.5 with Re=10,000, Pr=0.71, Gr=10^6 and AR=1

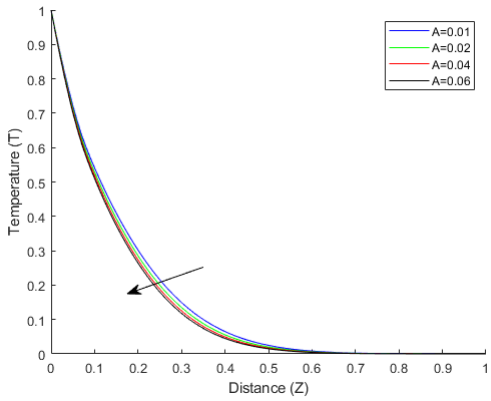

Fig. 9. The Temperature profiles for various values of A at X=0.5,Y=0.5 with Re=10,000, Pr=0.71, Gr=10^6 and AR=1

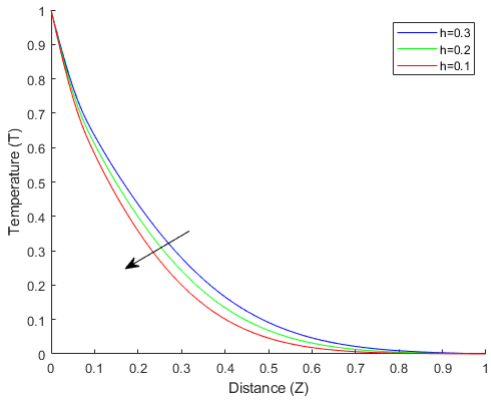

Fig. 10. The Temperature profiles for various values of h at X=0.5,Y=0.5 with Re=10,000, Pr=0.71, Gr=10^6 and AR=1

3 . A decrease in the distance between the fan and the greenhouse floor decrease the temperature profiles.

4 . A decrease in the distance between the air inlet position and the greenhouse floor decrease the temperature profiles.

5 . An increase in the Prandtl number leads to an increase in temperature profiles.

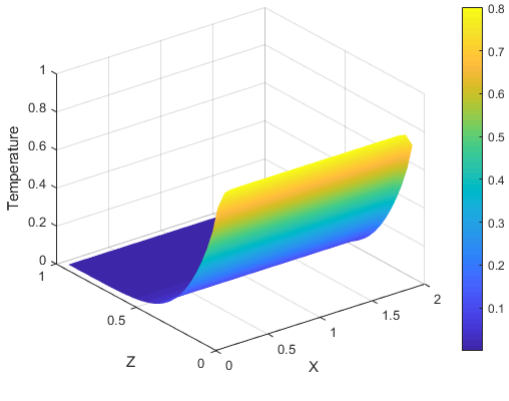

Fig. 11. The Temperature surface plot at Y=0.5 with Re=10,000, Pr=0.71, Gr=10^6 and AR=0.5

Acknowledgements

The author(s) highly appreciate the Pan African University, Institute for Basic Sciences, Technology, and Innovation for funding and support of this research project.

References

[1] S. Wang and T. Boulard, Journal of agricultural engineering research **75**, 27 (2000).
[2] J. Roy and T. Boulard, in *International Conference on Sustainable Greenhouse Systems-Greensys2004 691* (2004), pp. 457–464.
[3] H. Moriyama, C. Kubota, K. Kurata, M. Hayashi, N. Sabeh, P. Romero, G. A. Giacomelli, S. Sase, and M. Ishii, in *International Symposium on Greenhouse Cooling 719* (2006), pp. 385–392.
[4] E. Rico-Garcia, J. Reyes-Araiza, and G. Herrera-Ruiz, in *International Symposium on Greenhouse Cooling 719* (2006), pp. 325–332.
[5] S. O. Khaoua, P. Bournet, C. Migeon, T. Boulard, and G. Chasseriaux, Biosystems Engineering **95**, 83 (2006).
[6] G. Singh, P. P. Singh, P. P. S. Lubana, and K. Singh, Renewable Energy **31**, 1541 (2006).
[7] E. Rico-Garcia, I. Lopez-Cruz, G. Herrera-Ruiz, G. Soto-Zarazua, and R. Castaneda-Miranda, JApSc **8**, 4543 (2008).
[8] M. Teitel, O. Liran, J. Tanny, and M. Barak, Biosystems Engineering **101**, 111 (2008).
[9] S. Sengar and S. Kothari, African Journal of Mathematics and Computer Science Research **1**, 001 (2008).
[10] V. P. Sethi, Solar Energy **83**, 21 (2009).
[11] E. Rico-García, G. Soto-Zarazúa, O. Alatorre-Jacome, G. De la Torre-Gea, and D. Gomez-Melendez, International Journal of Physical Sciences **6**, 6541 (2011).
[12] J. Flores-Velazquez, J. I. Montero, E. J. Baeza, and J. C. Lopez, International Journal of Agricultural and Biological Engineering **7**, 1 (2014).
[13] A. Raczek and E. Wachowicz, Agricultural Engineering **149**, 185 (2014).
[14] X. He, J. Wang, S. Guo, J. Zhang, B. Wei, J. Sun, and S. Shu, Computers and Electronics in Agriculture **149**, 16 (2018).
[15] A. E. Newir and M. Ibrahim, European Journal of Engineering and Formal Sciences **2**, 107 (2018).
[16] E. Santolini, B. Pulvirenti, S. Benni, L. Barbaresi, D. Torreggiani, and P. Tassinari, Computers and Electronics in Agriculture **149**, 41 (2018).
[17] C.-R. Chu and T.-W. Lan, Biosystems Engineering **186**, 279 (2019).
[18] E. A. Villagran Munar and C. R. Bojacá Aldana (2020).
[19] S. Ghani, E. M. A. A. El-Bialy, F. Bakochristou, M. Mohamed Rashwan, A. Mohamed Abdelhalim, S. Mohammad Ismail, and P. Ben, Science and Technology for the Built Environment **26**, 141 (2020).
[20] H. Fatnassi, T. Boulard, C. Poncet, and M. Chave, Biosystems Engineering **93**, 301 (2006).
[21] J. C. Slattery, Chemical Engineering Education **6**, 174 (1972).
[22] F. Lai and F. Kulacki, International Journal of Heat and Mass Transfer **33**, 1028 (1990).
[23] D. C. Wilcox et al., *Turbulence modeling for CFD*, vol. 2 (DCW industries La Canada, CA, 1998).
[24] H. K. Versteeg and W. Malalasekera, *An introduction to computational fluid dynamics: the finite volume method* (Pearson education, 2007).